AFRL-ML-WP-TP-2006-468

EFFECT OF INITIAL TEMPER ON THE MECHANICAL PROPERTIES OF FRICTION STIR WELDED Al-2024 ALLOY (PREPRINT)

V. Dixit, R.S. Mishra, R.J. Lederich, and R. Talwar

SEPTEMBER 2006

Approved for public release; distribution is unlimited.

STINFO COPY

MATERIALS AND MANUFACTURING DIRECTORATE
AIR FORCE RESEARCH LABORATORY
AIR FORCE MATERIEL COMMAND
WRIGHT-PATTERSON AIR FORCE BASE, OH 45433-7750

REPORT DOCUMENTATION PAGE

Form Approved
OMB No. 0704-0188

1. REPORT DATE *(DD-MM-YY)*	2. REPORT TYPE	3. DATES COVERED *(From - To)*
September 2006	Journal Article Preprint	

4. TITLE AND SUBTITLE
EFFECT OF INITIAL TEMPER ON THE MECHANICAL PROPERTIES OF FRICTION STIR WELDED Al-2024 ALLOY (PREPRINT)

5a. CONTRACT NUMBER
FA8650-04-C-5704

5b. GRANT NUMBER

5c. PROGRAM ELEMENT NUMBER
78011F

6. AUTHOR(S)
V. Dixit and R.S. Mishra (University of Missouri-Rolla)
R.J. Lederich and R. Talwar (The Boeing Company)

5d. PROJECT NUMBER
2865

5e. TASK NUMBER
25

5f. WORK UNIT NUMBER
25100000

7. PERFORMING ORGANIZATION NAME(S) AND ADDRESS(ES)
University of Missouri-Rolla
Department of Materials Science and Engineering
Center for Friction Stir Processing
B. 37 McNutt Hall
1870 Miner Circle
Rolla, MO 65409-0340

The Boeing Company
Phantom Works
Advanced Manufacturing R&D
St. Louis, MO 63166

8. PERFORMING ORGANIZATION REPORT NUMBER

9. SPONSORING/MONITORING AGENCY NAME(S) AND ADDRESS(ES)
Materials and Manufacturing Directorate
Air Force Research Laboratory
Air Force Materiel Command
Wright-Patterson AFB, OH 45433-7750

10. SPONSORING/MONITORING AGENCY ACRONYM(S)
AFRL-ML-WP

11. SPONSORING/MONITORING AGENCY REPORT NUMBER(S)
AFRL-ML-WP-TP-2006-468

12. DISTRIBUTION/AVAILABILITY STATEMENT
Approved for public release; distribution is unlimited.

13. SUPPLEMENTARY NOTES

This paper was submitted to Science and Technology of Welding and Joining (STWJ), published by the Institute of Materials, Minerals and Mining. PAO Case Number: AFRL/WS 06-2073, 25 Aug 2006.

14. ABSTRACT
The microstructural evolution and resultant mechanical properties during friction stir welding (FSW) of precipitation strengthened aluminum alloys depend on initial temper as well as FSW process parameters. Al-2024 alloy under two different initial tempers, T3 and T8, was used in this study. FSW bead-on-plate runs were performed at different values of process parameters (tool rotation rate and tool traverse speed). Microstructure and mechanical properties of the nugget region and heat affected zone (HAZ) were evaluated. Differential scanning calorimetry (DSC) revealed that in the nugget region, presence of GPB zone results from the partial dissolution of Al2CuMg phase. The microstructure and tensile properties were found to be independent of the initial temper of the material in the nugget region. In the HAZ region, tensile properties increased at higher heat-index values for T3 condition, and decreased monotonically for T8 condition.

15. SUBJECT TERMS
aluminum alloys, welding, differential scanning calorimetry, microstructural evolution, tensile strength

16. SECURITY CLASSIFICATION OF:			17. LIMITATION OF ABSTRACT:	18. NUMBER OF PAGES	19a. NAME OF RESPONSIBLE PERSON (Monitor)
a. REPORT	b. ABSTRACT	c. THIS PAGE			Mary E. Kinsella
Unclassified	Unclassified	Unclassified	SAR	24	19b. TELEPHONE NUMBER *(Include Area Code)* N/A

Effect of initial temper on the mechanical properties of friction stir welded Al-2024 alloy

V. Dixit[1], R. S. Mishra[1,*], R. J. Lederich[2] and R. Talwar[2]

Abstract

The microstructural evolution and resultant mechanical properties during friction stir welding (FSW) of precipitation strengthened aluminum alloys depend on initial temper as well as FSW process parameters. Al-2024 alloy under two different initial tempers, T3 and T8, was used in this study. FSW bead-on-plate runs were performed at different values of process parameters (tool rotation rate and tool traverse speed). Microstructure and mechanical properties of the nugget region and heat affected zone (HAZ) were evaluated. Differential scanning calorimetry (DSC) revealed that in the nugget region, presence of GPB zone results from the partial dissolution of Al_2CuMg phase. The microstructure and tensile properties were found to be independent of the initial temper of the material in the nugget region. In the HAZ region, tensile properties increased at higher heat-index values for T3 condition, and decreased monotonically for T8 condition.

Keywords: Aluminum alloys, Welding, Differential scanning calorimetry, Microstructural evolution, Tensile strength

[1] Center for Friction Stir Processing, Department of Materials Science and Engineering, University of Missouri, Rolla, MO 65409, USA

[2] Advanced Manufacturing R&D, Boeing - Phantom Works, St. Louis, MO 63166, USA

[*] Corresponding author. E-mail: rsmishra@umr.edu

Introduction

High strength Al-Cu-Mg based precipitation strengthened alloys such as Al-2024 have found extensive applications in aerospace industry. These alloys are difficult to weld by traditional fusion welding method because of hot-cracking. Moreover, the material experiences an enormous reduction in strength because of the formation of dendritic structure in the welded region. FSW has emerged as an attractive technique for the welding of such alloys.[1] It is a solid state welding process, which eliminates solidification defects and significantly reduces residual stresses at the joints. In addition, microstructural modification of the welded region leads to better retained baseline mechanical properties. Solid state joining is made possible by the generation of localized frictional heat and high deformation of material around the tool. These thermo-mechanical conditions are governed by process parameters. Specifically, peak temperature is found to depend predominantly on tool rotation speed (ω) and tool traverse speed (v). This relationship has been represented in terms of pseudo heat-index (HI) where,[2]

$$HI = \frac{\omega^2}{v \times 10^4} \qquad (1)$$

where ω is in number of rotations per minute (rpm) and v is in inch per minute (ipm).

Peak-temperature increases with increase in HI, which lowers the flow-stress and facilitates the material flow.[3] Any non-conformity in material flow around the rotating tool generates defects in the friction stirred region.[4]

Important features of the microstructural evolution in the friction stir welded Al-2024 alloy are well established. Localized thermo-mechanical conditions determine the grain structure development and precipitation of strengthening particles in the nugget region. The microstructural studies in friction stir welded Al-2024 has revealed the presence of mainly fine, fully recrystallized and some large partially recrystallized grains consisting of sub-grains.[5]

Quantitative analysis has shown that initial temper does not influence the microstructure in the nugget region for the given processing condition.[6] This region involves the formation of GPB zone at the expense of partial dissolution of Al_2CuMg (S phase) precipitates. Study also showed that properties in the HAZ region depend immensely on the initial temper of parent material. The hardness value at HAZ was found to be higher than at nugget.[6-9] The digital image correlation (DIC) technique has identified thermo-mechanically affected zone (TMAZ) /nugget interface as the weakest region of the joint, irrespective of the initial temper.[6,9]

Most of the previous studies have thus far, focused on studying the microstructural evolution across the friction stirred region at a chosen set of processing conditions. The present study aims to understand the influence of initial temper on the microstructural evolution and tensile strength across the friction stirred region at different HI values.

Experimental procedure

For this study, commercial 0.125” thick sheets of Al-2024 at two different “as received” initial tempers, T3 and T8, were used. Sheets were friction stir welded using bead-on-plate configuration at different HI values, namely, 2.5, 3.6, 6.4, 6.6 and 10. Experimental setup involved the usage of steel back-up plate and 0° angle of tilt because of scrolled shoulder of the FSW tool. The processed samples were kept at room temperature for natural ageing to allow for the microstructural stabilization.

Microstructural observations were done using optical microscopy (OM) and transmission electron microscopy (TEM). For TEM, 3 mm thin discs were sectioned from the nugget, HAZ and unprocessed region. These discs were thinned and polished on SiC grit till they were 100 μm thick and then electro-polished using Struers Tenupol-2 twin-jet electro-polisher. The electrolyte

used was 20% HNO_3+80% CH_3OH mixture at -35°C. Modified Keller's reagent (150 ml water, 3 ml nitric acid and 6 ml hydrofluoric acid) was used as an etchant for OM. Microstructural defects in the nugget region were observed using JEOL-840 scanning electron microscope (SEM). Qualitative study of precipitation was done using DSC. DSC measurements of processed samples were done on 2010 DSC V4.4E equipment at the heating rate of 10°C/minute in the range of 45°C to 550°C. The samples were sectioned from the relevant regions (nugget and HAZ) in the form of 3 mm disc, and weighed close to 15 mg.

Tensile properties were measured at nugget, HAZ and unprocessed regions along the welding direction using mini-tensile geometry at an initial stain rate of $1\times10^{-3}s^{-1}$.

Results

Unprocessed Al-2024 alloy (both in T3 and T8 initial tempers) consists of large pancake shaped grains (Fig. 1). In peak-aged 'T6' or 'T8' material, the presence of fine S phase precipitates aligned in <100> direction has been reported, while naturally aged 'T3' material consists of GPB zone.

TEM micrographs of the nugget region (Fig. 2) show the presence of dynamically recrystallized grains with high angle grain boundaries. Most of the grains were fine and free of dislocation structures. The exact mechanism of dynamic recrystallization is still in debate.[11] Though large variation in grain-size was observed, evidently, increase in HI values appeared to coarsen the grain structures in the nugget region. It was also observed that at low HI, the area fraction (thus, volume fraction) of these precipitates is large, which appeared to decrease at higher HI. Similarly, coarsening of second phase particles was also observed (Fig. 3) at higher HI. These coarse S phase precipitates were found to be homogenously distributed in the matrix

in this region. At low HI, the presence of worm-hole defects and micro-voids was observed (Fig. 4 and Fig. 5) predominantly on the advancing side of the nugget region of the friction stirred samples. Largest worm-hole defects were present at the interface of the pin-bottom and material and its dimensions decreased at higher HI values. Thermal conditions for HI $\geq$ 6.4 generated defect-free welds.

DSC curves have extensively been used for the study of solid state reactions in precipitation strengthened aluminum alloys.[6,12-18] For Al-2024 alloy in T3 temper, its DSC plot (Fig. 6) shows four distinct regions, [13]

(a) dissolution of GPB zone (between 150°C and 235°C),

(b) formation of S phase (between 235°C and 300°C),

(c) formation of Al_2Cu (θ) phase and dissolution of S phase (between 300 and 500°C), and

(d) incipient melting (around 505°C).

DSC plot of peak aged material showed the presence of some amount of GPB zone; however the peak areas of regions (a) and (b) were much smaller as compared to that of naturally aged one. DSC curves did not indicate the presence of any significant phase other than GPB zone and S phase. Although, previous studies have reported the existence of θ phase but its amount is quite small in comparison to that of GPB zone and S phase.[12] Fe and Mn based dispersoids do not undergo any transformation and cannot contribute to the heat effects.

Peak areas of regions (a) and (b) correspond to the amount of GPB zone present in the material and formation of S phase from GPB zone respectively. In case of friction stirred T3 material, the DSC plot of the nugget (Fig. 7) of the sample processed at HI=1.6 showed negligible peak area of region (a), which increased at higher HI. Correspondingly, the peak area of region (b) increased. It indicated an increase in the volume fraction of GPB zone with increase

in thermal input. Corresponding decrease in the volume fraction of S phase precipitates is shown by the microstructural observations in TEM studies.

Effect of initial temper appeared to exist mainly in the HAZ of the friction stirred specimens. In the processed T3 material, extremely fine S phase precipitates aligned in <100> directions were observed, similar to those originally present in parent T8 material (Fig. 8b). DSC plots and TEM studies show that the volume fraction of these precipitates increase at higher HI. No visible alteration in grain-structures was registered because of short thermal cycle and absence of mechanical deformation in this region.

In the nugget region, the tensile properties were found to be independent of the initial temper (Fig. 9). However, in the HAZ region, tensile strength increased at higher HI values for friction stirred T3 material, and exhibited the opposite trend for the T8 material (Fig. 10). It was also noted that properties in the HAZ region of the processed T3 material were significantly higher than corresponding tensile properties at nugget and unprocessed regions for both initial tempers. A relatively small variation in tensile strength values was observed at different HI values in all the regions of interest.

Discussion

Process parameters determine the thermo-mechanical conditions during FSW, which critically influence the microstructural evolution and mechanical deformation. Low peak temperature at low HI values increases the flow stress of the material and makes the plastic deformation difficult.[2] The tool-pin translation vector becomes opposite to the tool rotation vector and offers higher resistance to the material flow on the advancing side. At the pin bottom, peak temperature is least because of small pin surface area. In addition, its proximity to the back-

up plate decreases the extent of heat retention. These factors make these two locations the preferred sites for the formation of defects, as observed in this study.

Higher HI values increase the thermal cycle of the work-piece during FSW. In the nugget region of the processed T3 material, the negligible peak area of region ‘a’ observed at HI=1.6 (Fig. 4) confirms that even at such small thermal cycle, peak temperature is high enough to completely transform GPB zone into S phase. Moreover, increase in the peak area of this region at higher HI confirms that GPB zone in the nugget region is formed as a result of partial dissolution of S phase. Also, the peak temperature in this region crosses the solvus temperature of S phase at all HI values considered. However, the small volume fraction of fine S phase indicates that the fast cooling of the processed region does not allow the re-precipitation of S phase at such small thermal input. The first distinct indication of bi-modal size distribution of S phase is observed for HI=6.4. For higher HI values, the complex kinetics of formation and dissolution of both S phase and GPB zone governs the eventual microstructural evolution in the nugget region. These observations are consistent for both T3 and T8 initial tempers. The difference in the precipitation evolution for these two tempers is the heat-effect of the transformation of GPB zone to S phase, which can be assumed negligible because of its fast kinetics of transformation. All these factors confirm that microstructural characteristics in the nugget region are independent of the initial temper of the material for the range of process parameters considered. Grain coarsening at higher HI values is likely to be helped by high peak temperature and decrease in the volume fraction of second phase particles, which lowers the extent of grain boundary pinning.

For the processed T3 material, DSC plots and TEM micrographs indicate that higher thermal input leads to transformation of higher amount of GPB zone into S phase in the HAZ

region. It also confirms that peak temperature does not exceed the solvus temperature of the S phase in this region. For the parent T8 material, thermal cycle decreased the volume fraction of residual GPB zone (Fig. 6). In addition to process parameters, precipitation in the HAZ region is also governed by the relative distance from the nugget region. For example in TMAZ, higher extent of coarsening is observed (Fig. 8). Previous studies have shown that coarsening of S phase with decrease in distance from the nugget leads to the decrease in the hardness values.[6,7]

Presence of residual GPB zone in parent T8 material explains the lower strength values of the as received peak aged material. T3 material expectedly has the lowest tensile strength, in which, GPB zone is the main strengthening phase. Grain structures contribute little to the strength because of large grain-size. Precipitation of uniformly distributed extremely fine S phase at the expense of GPB zone has been shown to impart high tensile strength at the HAZ region.[6,9] In case of the processed T8 material, however, coarsening of the S phase precipitates decreases the strength at higher HI values.[6] Here, an unexpected increase in tensile strength at HI=6.4 occurs probably because of the transformation of residual GPB zone into S phase precipitates.

In the nugget region, the major contribution to the strength is given by S phase and GPB zone. In addition, the presence of fine equiaxed grains also significantly contributes to the strength.[6] The generation of GPB zone at the expense of coarse S phase precipitates at higher HI values corresponds to, and probably explains the increase in tensile properties in this region.

Conclusions

1. In the nugget region, the initial temper does not significantly influence the microstructural evolution at all HI values, and the presence of GPB zone in the nugget confirms that peak-

temperature crosses the solvus temperature of S phase precipitates even at low HI.

2. In the HAZ region, for the T3 initial temper, volume fraction of GPB zone decreases at higher HI, and peak temperature does not cross the solvus temperature of S phase at HAZ for the range of HI values considered.
3. At low HI values, formation of worm-hole defect occurs predominantly on the advancing side of the nugget and at the interface of pin bottom and material because of insufficient plastic flow. Size of worm hole defects decrease at higher HI and above HI=6.4, defect free welds were generated.
4. Tensile properties in the HAZ region are higher than those in the nugget region, both of which increase at higher HI values for T3 material. However, for the T8 material, tensile properties at HAZ show a decreasing trend.

Acknowledgements

The authors gratefully acknowledge the Center for Aerospace Manufacturing financial support provided by the Air Force Research Laboratory through contract no. FA8650-04-C-704.

References

1. W. M. Thomas: ‘Friction stir butt welding’, International Patent App. No. PCT/GB92/02203 and GB Patent App. No. 9125978.8, Dec. 1991, U.S. Patent No. 5460317.
2. W. J. Arbegast: ‘Modeling friction stir joining as a metal working process’, Hot Deformation of Aluminum Alloys III, TMS, 2003, 313.
3. C. M. Sellars and W. J. MC G. Tegart: Int. Met. Rev., 1972, **17**, 1.
4. W.J. Arbegast: “Technology gaps that stand in the way of taking friction stir to an industrial standard’, SAE Friction Stir Welding Symposium, Albuquerque, New Mexico, June 10-11, 2004.
5. M. Karlsen, ∅. Frigaard, J. Hjelen, ∅. Grong and H. Norum: ‘SEM-EBSD characterization of the deformation microstructure in friction stir welded 2024 T351 aluminum alloy’, Materials Science Forum, 2003, **426-432**, 2861.
6. C. Genevois, A. Deschamps, A. Denquin and B. Doisneau-cottignies: ‘Quantitative investigation of precipitation and mechanical behavior of AA2024 friction stir welds’, Acta Materialia, 2005, **53**, 2447.
7. M.J. Jones, P. Heurtier, C. Desrayaud, F. Montheillet, D. Allehaux and J. H. Driver: ‘Correlation between microstructure and microhardness in a friction stir welded 2024 aluminium alloy’, Scripta Materialia (2005), **52**, 693.
8. J. C. Ehrström, A. Bigot, L. Cervi, H. Gerard: ‘Microstructure and properties of aluminum alloys friction stir welds for aircraft application’, Materials Science Forum, 2003, **426-432**, 2941.

9. P. Heurtier, M.J. Jones, C. Desrayaud, J. H. Driver and F. Montheillet: 'Thermomechanical conditions and resultant microstructures in friction stir welded 2024 aluminum', Materials Science Forum, 2003, **426-432**, 2927.

10. W. D. Lockwood, B. Tomaz and A. P. Reynolds: 'Mechanical response of friction stir welded AA2024: experiment and modeling', Materials Science and Engineering A, 2002, **323**, 348.

11. R.S. Mishra, Z.Y. Ma: 'Friction stir welding and processing', Materials Science and Engineering R, 2005, **50-8**.

12. M. J. Starink, S. C. Wang and I. Sinclair: 'A model for local proof strength of 2xxx welds', Friction Stir Welding and Processing III, TMS, 2005, 233.

13. M. J. Starink and Jialin Yan: 'A model for strengthening of Al-Cu-Mg alloys', Proceedings from 1st International Symposium on Metallurgical Modeling for Aluminum Alloys, 13-15 Oct. 2003, Pittsburgh, PA, ASM international, 2003.

14. M. J. Starink and P. J. Gregson: 'A quantitative interpretation of DSC experiments on quenched and aged SiC_p reinforced 8090 alloys', Scripta Materialia., 1995, **33-6**, 893.

15. N. Gao, L. Davin, S. Wang, A. Cerezo and M. J. Starink: 'Precipitation in stretched Al-Cu-Mg alloys with reduced alloying content studied by DSC, TEM and atom probe', Materials Science Forum, 2002, **396-402**, 923.

16. M. J. Starink, N. Gao, M. Furukawa, Z. Horita, C. Xu and T. G. Langdon: 'Microstructural developments in a spray-cast Al-7034 alloy processed by equal-channel angular pressing', Rev. Adv. Mat. Sci., 2004, **7**, 1.

17. C. Badini, F. Mario and E. Verné: 'Calorimetric study on precipitation path in 2024 alloy and its SiC composite', Materials Science and Engineering A, 1995,**191**,185.

18. M. J. Starink: ‘Analysis of aluminum based alloys by calorimetry: quantitative analysis of reactions and reaction kinetics’, International Materials Reviews, 2004, **49**, 191.

Figures

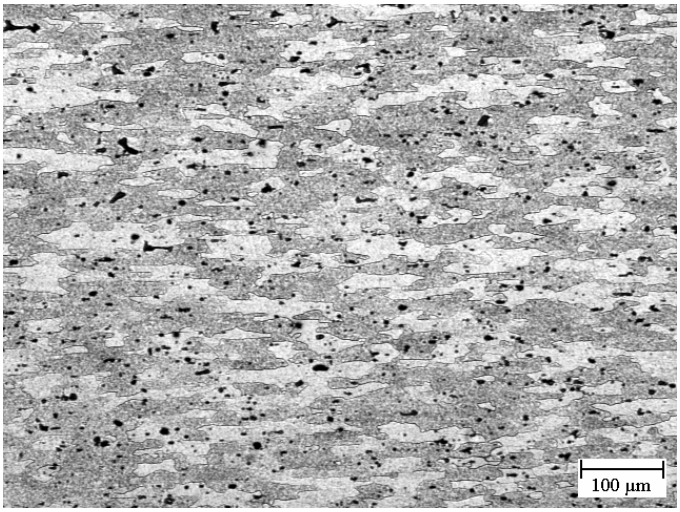

Fig. 1 Optical micrograph of unprocessed material shows large pancake shaped grains.

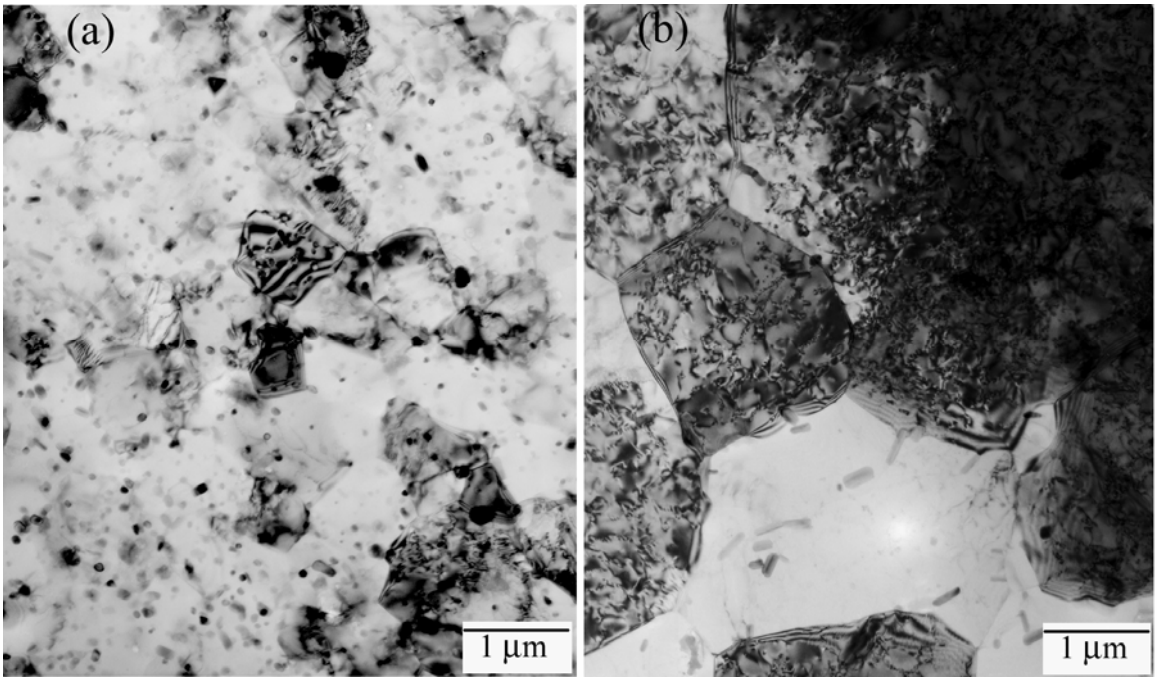

Fig. 2 Bright field TEM micrographs show microstructure in the nugget region for (a) HI=2.5 and (b) HI=10, which indicate grain-coarsening at higher HI values.

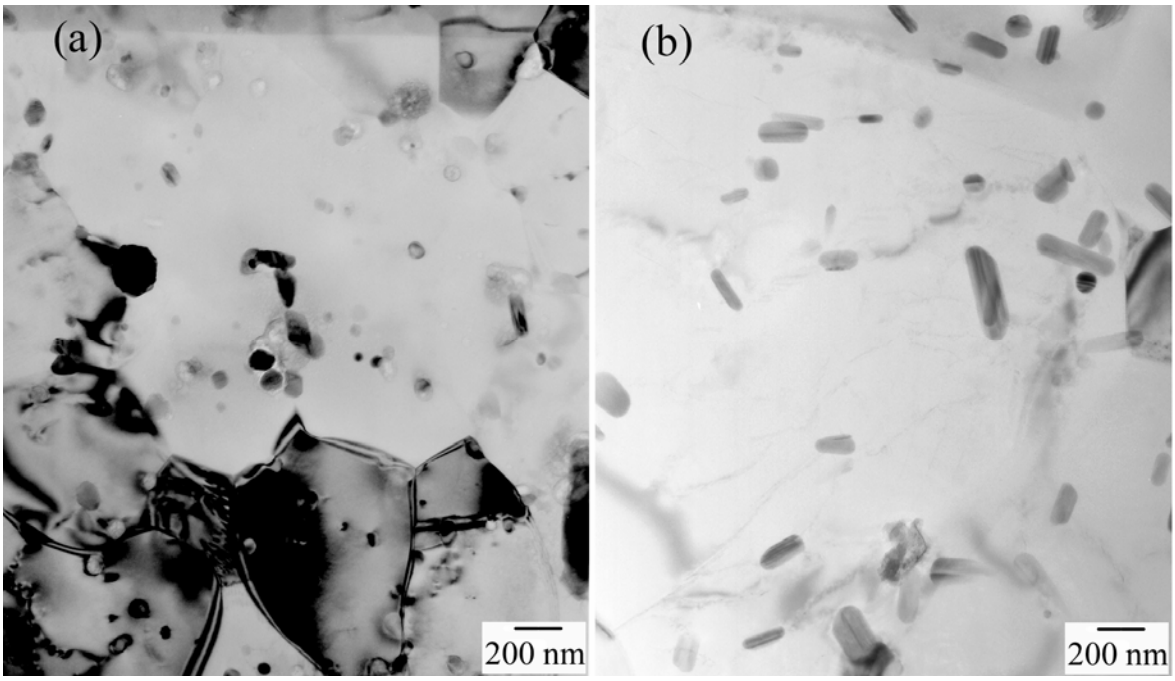

Fig. 3 Precipitate size for (a) HI=2.5 is smaller than that for (b) HI=6.6 in the nugget.

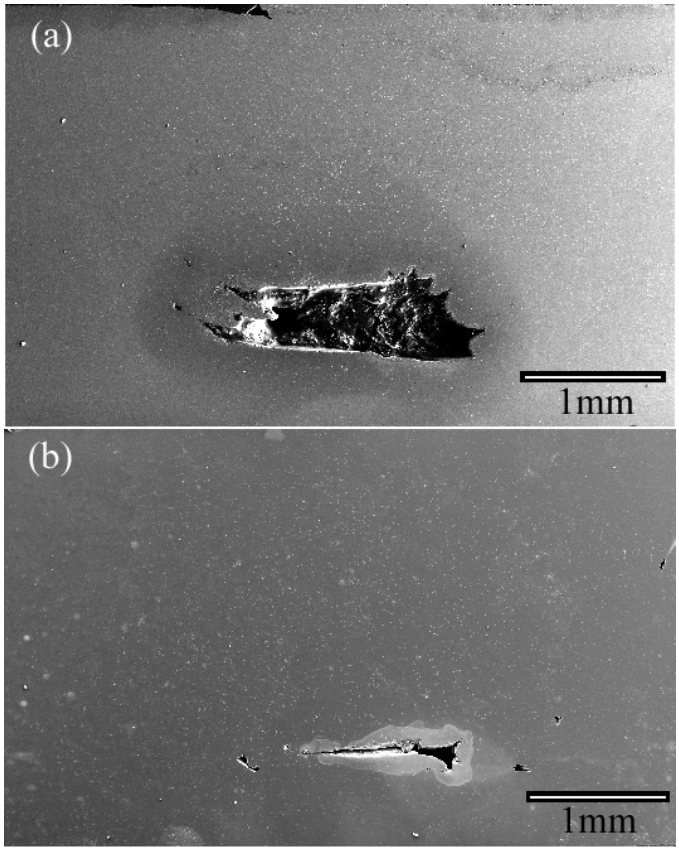

Fig. 4 Worm-hole defect in nugget of the samples processed at, (a) HI=2.5 and (b) HI=3.6.

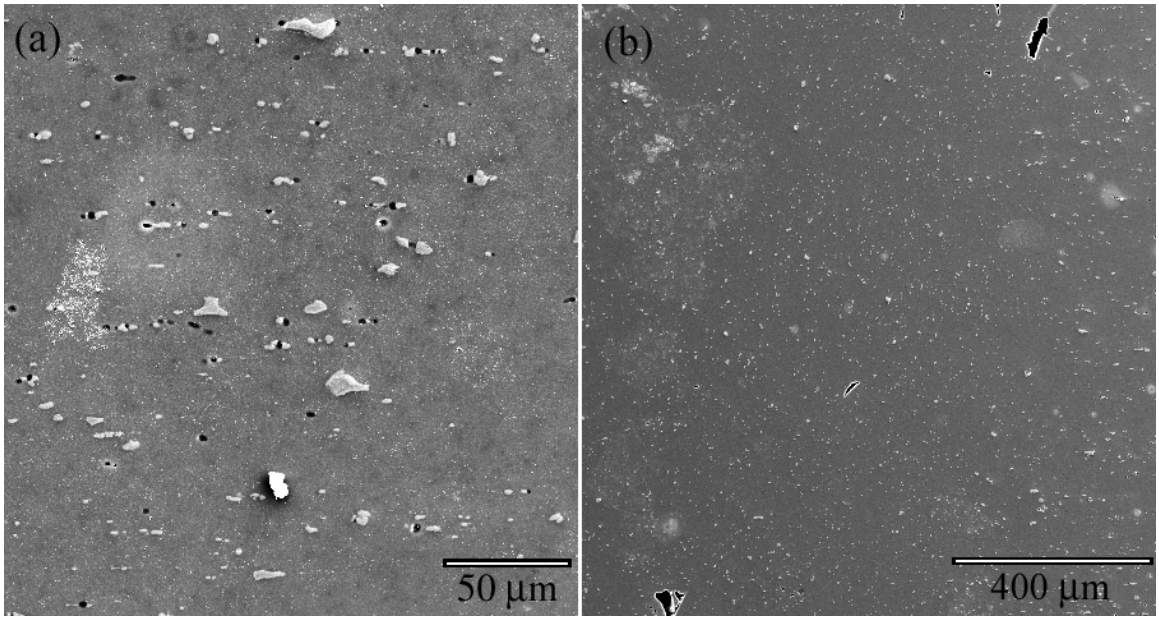

Fig. 5. Parent region shows particle drop-outs (shown in (a)), which are different from the defects present on the advancing side (shown in (b)) of the sample processed at HI=3.6.

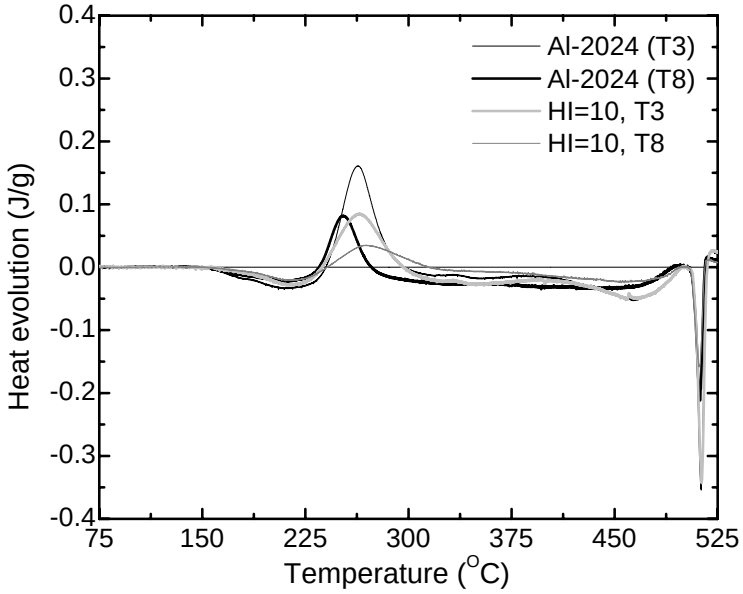

Fig. 6 DSC plot of Al-2024 (T3) alloy shows four distinct regions.

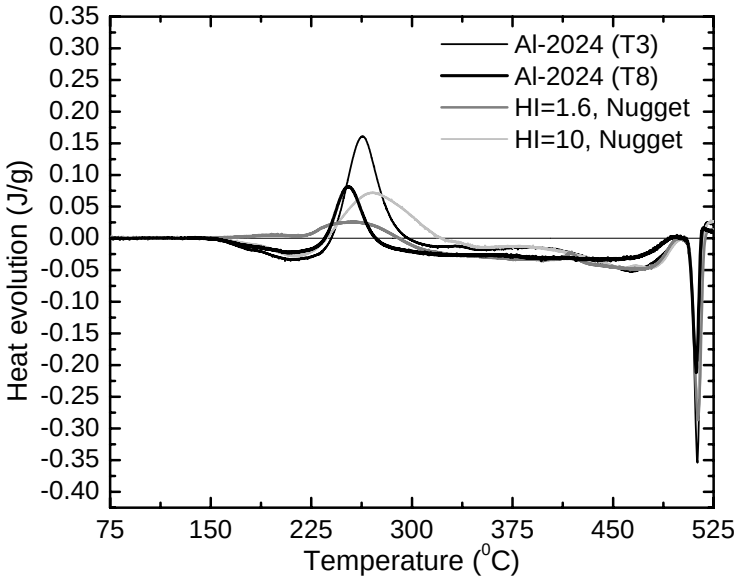

Fig. 7 In the nugget region, thermal cycle is high enough to completely transform GPB zone to S phase for HI≥1.6.

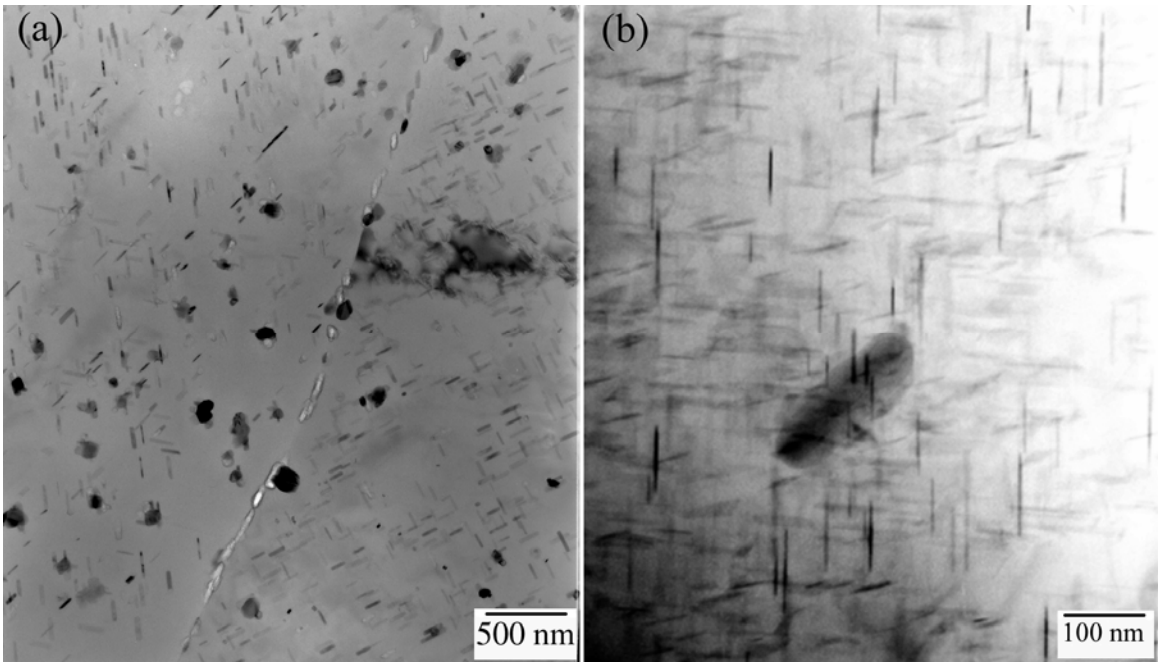

Fig. 8 Precipitate coarsening is more in the (a) TMAZ region as compared to in the (b) HAZ region.

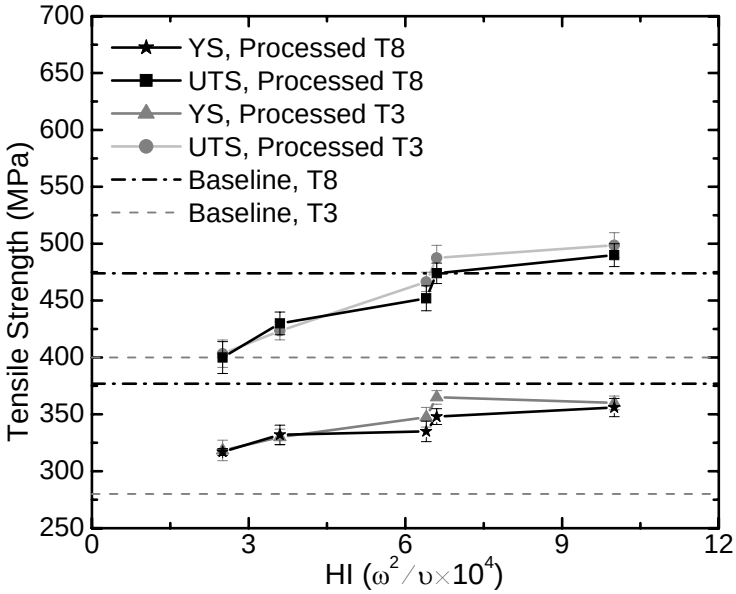

Fig. 9 Tensile strength in the nugget region increases at higher HI, and is independent of the initial temper of the material.

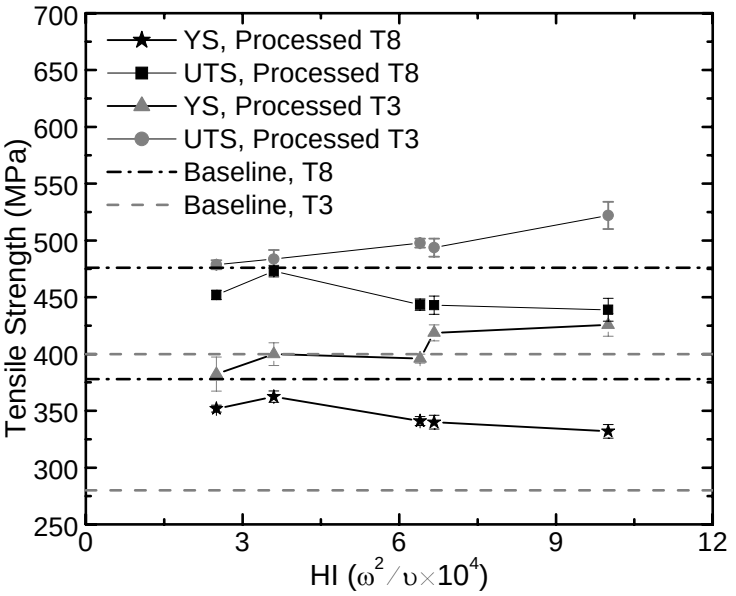

Fig. 10 Tensile strength values in the HAZ region show opposite trends for T3 and T8 initial tempers.